Journal of Engineering Mathematics **31:** 59–80, 1997.

Geometrical effects in a Joule heating problem from miniature soldering

S.W. RIENSTRA
Department of Mathematics and Computing Science, Eindhoven University of Technology, P.O. Box 513, 5600 MB Eindhoven, The Netherlands

Received 13 December 1994; accepted in revised form 6 February 1996

Abstract. The soldering of small, delicate electronic devices by means of a blade thermode (a small, thin, rectangular ⊔- or ⊔⊔-shaped soldering iron) requires the lower side of the thermode to have a uniform temperature distribution. This is not easily obtained: during start-up the corners tend to be too hot, and too cold in the stationary phase. In the present study the various aspects that determine the heat flow and the temperature distribution are analysed, both for the dynamic and the stationary cases.

For a temperature-independent (linear) material, approximate solutions are obtained for the dynamic problem. For the stationary problem, an exact solution is utilized that includes temperature-dependent (nonlinear) material. Practical design rules based on these solutions are proposed. The analysis compares very well with a numerical finite-element simulation.

Key words: soldering, heat transfer, Joule heating, conformal mapping, thermode.

1. Introduction

The soldering of electronic devices, like integrated circuits ("chips"), on a print board is known as miniature, subminiature, and micro-soldering. It is usually done by application of a ⊔- or ⊔⊔-shaped piece of metal, called a thermode. This thermode is electrically heated up to about 300°C (this varies with the application), while it is positioned with its lower side onto the pins or connectors to be soldered. Consider, for clarity, the following U-shaped geometry with ends indicated by A and D and corners indicated by B and C:

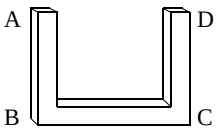

An electric potential difference is applied at the ends A and D. This induces a current that heats up the thermode according to Joule's law. The soldering takes place along side B-C. The basic question motivating the present study is:

> How to keep the temperature along the side B-C as *uniform* as possible, in order to avoid damage of the electronic circuits from excessive heating, while at the same time preventing incomplete soldering of the connectors by insufficient heating.

To answer this question we have to solve the combined problem of Ohmic heating and heat conduction. This problem is non-stationary since in each soldering cycle the usual procedure involves:

– a cool thermode at the start,
– a high current during the initial heating to attain the operational temperature quickly,
– a low current during the final stage when this temperature level is to be maintained.

Experience has shown that it is difficult to obtain a uniform temperature profile. In the high-current stage the corners B and C are heated up much more than the other parts, leading to temperatures of about 350°C, which is 50°C too high. In the low-current stage the corners B and C cool off to a value of about 250°C, which is 50°C too low. This change is due to a change in the relative importance of heat generation as compared to heat conduction:

– during the high-current stage heat generation dominates, especially at the inner corners of B and C where the electric field has a singularity,
– during the low-current stage conduction dominates, in which case the cool ends A and D cause the temperatures at B and C to be lower.

To quantify these observations and to show what is the rôle of the parameters involved, we will analyse a mathematical model of a thermode, utilizing the symmetry and slenderness of the geometry, and assuming ideally insulated boundaries. In the dynamic case we assume linear physical relations (material properties independent of the temperature). In the stationary case, however, we will take advantage of a fortuitous exact solution of the nonlinear problem with temperature-dependent material.

The results relate the amount of excess heat due to the corner singularities in the initial value problem and the stationary problem to the material and geometry parameters, leading to possible rules for thermode design.

2. The model

An industrial thermode is typically made of molybdenum, a Hastelloy alloy, tungsten (wolfram) or nichrome, which are all good electrical conductors (homogeneous and isotropic), with the electric current density $\mathbf{j}$ and the electric field $\mathbf{E}$ satisfying Ohm's law $\mathbf{j} = \sigma\mathbf{E}$ (ref. [1, 2, 3, 4]). Further, σ is the electric conductivity, *i.e.* the inverse of the specific electric resistance $1/\sigma$. For the effectively stationary current flow, as we will have here, the conservation of electric charge leads to a vanishing divergence of the electric current density, $\nabla \cdot \mathbf{j} = 0$. The electric field $\mathbf{E}$ satisfies $\nabla \times \mathbf{E} = 0$, and therefore has a potential ϕ, with $\mathbf{E} = -\nabla\phi$, satisfying

$$\nabla \cdot (\sigma \nabla \phi) = 0. \tag{2.1}$$

By definition, the potential ϕ is defined up to an arbitrary constant. If required, any suitable constant may be added.

The heat dissipated as a result of the work done by the field per unit time and volume is given by Joule's law, and leads to the heat-source distribution

$$\mathbf{j} \cdot \mathbf{E} = \sigma |\nabla \phi|^2. \tag{2.2}$$

Since energy is conserved, the net rate of heat conduction and the rate of increase of internal energy are balanced by the heat source, which yields (ref. [5, 6]) the equation

$$\rho c \frac{\partial T}{\partial t} = k \nabla^2 T + \sigma |\nabla \phi|^2, \tag{2.3}$$

where T is the temperature, k the thermal conductivity, ρ the density and c the specific heat of the material.

The thermal conductivity is mildly dependent on temperature. For molybdenum it varies from $k = 142\,\mathrm{W/mK}$ at 21°C to $k = 120\,\mathrm{W/mK}$ at 300°C (ref. [7, 8]), so we further assume that k is a constant.

The electric conductivity σ is a material parameter which is quite strongly dependent on temperature. For example, for molybdenum it drops from $\sigma = 19 \cdot 10^6\,(\Omega\mathrm{m})^{-1}$ at 21°C to $8.0 \cdot 10^6\,(\Omega\mathrm{m})^{-1}$ at 300°C. Nevertheless, to make progress we will assume a constant σ, independent of T, in the dynamic (initial-value) problem. This, then, leads to the Laplace equation for ϕ

$$\nabla^2\phi = 0. \tag{2.4}$$

For the stationary problem, it was shown by Young [4, 9] that analytical progress is possible for the more general case of temperature-dependent σ and k. Exact solutions, especially when k is constant, may be obtained for metals, which in general satisfy the Weidemann-Franz-Lorenz law [10]

$$\frac{k(T)}{\sigma(T)} = \alpha T. \tag{2.5}$$

Here, T is the absolute temperature, and the Lorenz number α varies slightly from metal to metal [11]. (In addition, it may be noted that interesting questions with respect to uniqueness of the solution arise for other types of material [12, 13].)

For a constant k, it is very attractive, for reasons of accuracy, to introduce the relation

$$\frac{1}{\sigma(T)} = \beta(T - T_1). \tag{2.6}$$

For example, in the range $273\,\mathrm{K} < T < 1000\,\mathrm{K}$ the σ of molybdenum is very well described by Equation (2.6) with $\beta = 0.026 \cdot 10^{-8}\,\Omega\mathrm{m/K}$, and $T_1 = 89\,\mathrm{K}$. Since the analysis of Young is only trivially altered if we allow for an origin shift of the temperature, we will use here relation (2.6) for the stationary problem. At the same time, it is no longer necessary to let T denote absolute temperature.

As far as the other parameters are concerned, the density ρ is practically constant, and the specific heat c varies slightly. Typically, for molybdenum we have $c = 250\,\mathrm{J/kg\,K}$ at 21°C and $c = 275\,\mathrm{J/kg\,K}$ at 300°C. Therefore, henceforth it will also be taken constant.

We will simplify the geometry by using the inherent symmetry, so that we arrive at the L-shaped region

$$\Omega_L = \{(x, y) \mid (0 \le x \le a,\ 0 \le y \le L_a) \cup (0 \le x \le L_b,\ 0 \le y \le b)\}, \tag{2.7}$$

(Figure 1) with the cool end I and the hot end II.

Between end I and end II the potential difference is $\frac{1}{2}V$, while at the insulated boundaries the component of **E** normal to the boundary vanishes. Assuming that conduction and convection by the surrounding air and the soldering material is negligible, we observe that the normal heat flux vanishes at insulated boundaries, similar to the electric field.

At end I the thermode will remain at the temperature of the environment (the thermode holder) T_0, while at end II it assumes its maximum value. So we have along the boundaries

$$\phi = 0, \qquad T = T_0 \qquad \text{at end I,} \tag{2.8}$$

$$\phi = \tfrac{1}{2}V, \qquad \tfrac{\partial}{\partial x}T = 0 \qquad \text{at end II,} \tag{2.9}$$

$$\nabla\phi \cdot \mathbf{n} = 0, \qquad \nabla T \cdot \mathbf{n} = 0 \qquad \text{at the insulated boundaries,} \tag{2.10}$$

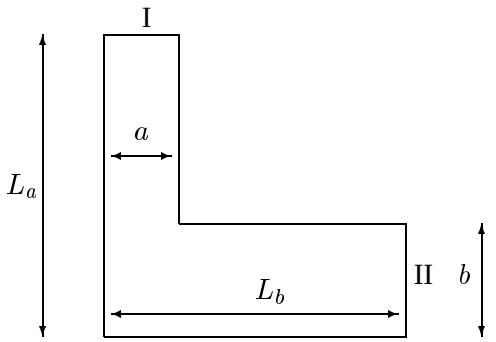

Figure 1. Sketch of geometry Ω_L

where **n** is normal to the boundary, and, of course, $T_0 > T_1$.

The typical thickness of a thermode is $d = 0.5\,\text{mm}$, which is small compared with a leg width of (the order of) 2 mm and a length of 20 mm. In view of Equations (2.10) we may therefore assume that both ϕ and T are constant in a cross-wise direction, making the problem geometrically two-dimensional.

The leg lengths L_a and L_b are in practice sufficiently larger than the widths a and b to justify the assumption that the electric field and the temperature field are practically one-dimensional near the ends I and II, in correspondence with the boundary conditions (2.8–2.10).

Initially, T is typically equal to room temperature, although in practice it may be somewhat higher. We assume here

$$T = T_0 \qquad \text{uniformly at} \quad t = 0. \tag{2.11}$$

Finally, Table 1 summarizes the common range of values of the physical quantities. This, among other things, will be useful later to determine the typical order of magnitude of the various dimensionless groups.

Table 1. Typical values of the problem parameters.

thickness d	0.5 mm		
length L_a, L_b	15 – 30 mm		
width a, b	1.5 – 2 mm		
temperature T	25 – 300°C, (corners 250 – 350°C)		
voltage V	0.1 – 2 V		
	molybdenum:	tungsten:	Hastelloy (typ.):
density ρ	10 200 kg/m^3	19 300 kg/m^3	9 000 kg/m^3
specific heat c	275 J/kg K	141 J/kg K	375 J/kg K
thermal conductivity k	120 W/mK	142 W/mK	13 W/mK
electric conductivity σ	$1 \cdot 10^7\ (\Omega\text{m})^{-1}$	$8 \cdot 10^6\ (\Omega\text{m})^{-1}$	$7 \cdot 10^5\ (\Omega\text{m})^{-1}$
Lorenz number α	$2.6 \cdot 10^{-8}\ (\text{V/K})^2$	$3.1 \cdot 10^{-8}\ (\text{V/K})^2$	$5.1 \cdot 10^{-8}\ (\text{V/K})^2$

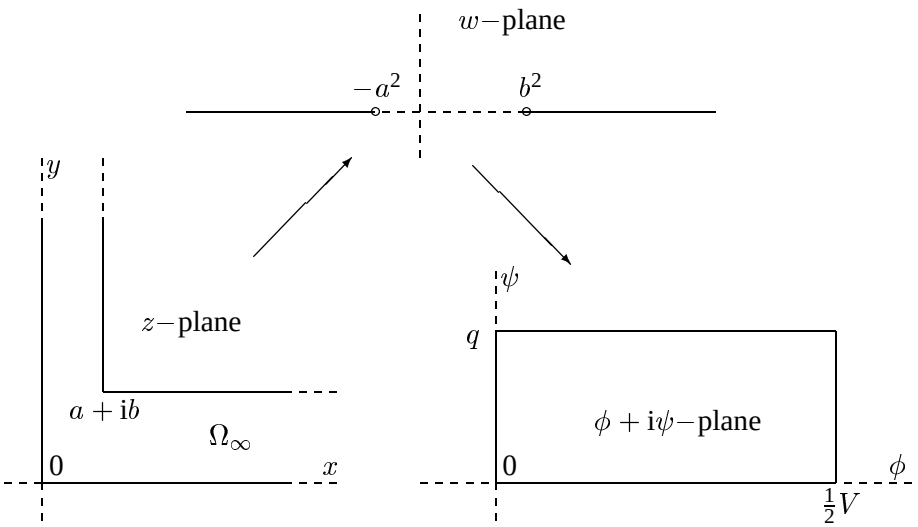

Figure 2. Complex $z = x + \mathrm{i}y$-plane mapped to the $\phi + \mathrm{i}\psi$-plane via the w-plane.

3. The electric field for constant σ

For constant σ the electric field is not coupled to the temperature field, and may therefore be found independently. Furthermore, as we will see later, this solution is not only relevant to the initial-value problem. The stationary solution with the temperature-dependent material (2.6) will be seen to be expressible in terms of this constant-σ field.

The solution for ϕ in Ω_L, with L_a and L_b finite, is difficult to derive. However, since L_a/a and L_b/b are sufficiently larger than 1, the solution is practically indistinguishable from a solution in

$$\Omega_\infty = \{(x, y) \mid (0 \le x \le a,\ 0 \le y < \infty\}) \cup (0 \le x < \infty,\ 0 \le y \le b)\}, \tag{3.1}$$

with the following behaviour:

$$\left.\begin{aligned} \frac{\partial \phi}{\partial y} &\to \text{constant} \qquad \text{for } \ y \to \infty, \ \ 0 \le x \le a, \\ \frac{\partial \phi}{\partial x} &\to \text{constant} \qquad \text{for } \ x \to \infty, \ \ 0 \le y \le b. \end{aligned}\right\} \tag{3.2}$$

This is because the lines $\phi =$ constant (the equipotential lines) in the legs quickly arrange themselves perpendicular to the boundaries, and thus allow the application of the condition $\phi = 0$ at end I and $\phi = \frac{1}{2}V$ at end II.

Now the solution can be derived by means of a relatively simple application of conformal mapping ([14, 15]), where we identify the physical (x, y)-plane with the complex z-plane via $z = x + \mathrm{i}y$. Using standard techniques (see Appendix A) we see that the following function, which is analytic in the upper complex half plane,

$$G(w) = \frac{2\mathrm{i}a}{\pi}\ \mathrm{artanh}\left(\frac{a\sqrt{b^2 - w}}{b\sqrt{a^2 + w}}\right) + \frac{2\mathrm{i}b}{\pi}\ \arctan\left(\frac{\sqrt{b^2 - w}}{\sqrt{a^2 + w}}\right) \tag{3.3}$$

defines the mapping

$$z = G(w) \tag{3.4}$$

that maps the upper half of the w-plane to Ω_∞ in the z-plane (Figure 2)[1]. Further details about its limiting behaviour, etc., may be found in Appendix A.

The final solution is obtained by positioning a point source of strength q (still to be determined) in $w = 0$, corresponding to a source (or sink, if we adopt a different sign convention) of electricity in $0 \le x \le a$, $y \to \infty$. The complex potential of this source in the w-plane is given by

$$F = \frac{q}{\pi}\log(w/b^2) + \phi_0, \tag{3.5}$$

where ϕ_0 is a constant yet to be determined. This constant is necessary for the problem as it has been posed, but has no direct physical relevance. (Finally, it will appear that $\phi_0 = \phi(0,0)$.) The complex potential $F = F(z)$ is now implicitly given by

$$z = G\left(b^2\,\mathrm{e}^{\pi q^{-1}(F-\phi_0)}\right). \tag{3.6}$$

The physical potential ϕ is given by the real part of F:

$$F(z) = \phi(x,y) + \mathrm{i}\psi(x,y), \tag{3.7}$$

where ψ, the imaginary part of F, is the conjugate of ϕ. The lines given by $\phi(x,y) =$ constant are called the equipotential lines. The applied potential is constant along the ends I and II, *i.e.* these ends coincide with equipotential lines. The lines given by $\psi(x,y) =$ constant are called the flux lines, the flux between two flux lines being constant. Insulated boundaries always coincide with flux lines. Thus we can choose $\mathrm{Im}(\phi_0) = 0$, so that

$$\begin{aligned} &\psi = 0 \quad \text{along} \quad \{x = 0,\ 0 \le y < \infty\} \cup \{0 \le x < \infty,\ y = 0\},\\ &\psi = q \quad \text{along} \quad \{x = a,\ b \le y < \infty\} \cup \{a \le x < \infty,\ y = b\}, \end{aligned} \tag{3.8}$$

while indeed $\phi(0,0) = \phi_0$. Furthermore, we can choose q and ϕ_0 such that

$$\begin{aligned} &\phi = 0 \quad \text{along} \quad \{0 \le x \le a,\ y = L_a\},\\ &\phi = \tfrac{1}{2}V \quad \text{along} \quad \{x = L_b,\ 0 \le y \le b\}, \end{aligned} \tag{3.9}$$

in the aforementioned approximate sense, for large enough L_a/a and L_b/b. Using the asymptotic results (A.4), we then obtain

$$\begin{aligned} q &= \frac{\frac{1}{2}V}{\dfrac{L_a}{a} + \dfrac{L_b}{b} - \dfrac{2}{\pi}\left(\dfrac{a}{b}\arctan\dfrac{a}{b} + \dfrac{b}{a}\arctan\dfrac{b}{a} + \log 4 - \log\Big(\dfrac{a}{b} + \dfrac{b}{a}\Big)\right)}\\ &\simeq \frac{\frac{1}{2}V}{L_a/a\ +\ L_b/b}, \end{aligned} \tag{3.10}$$

[1] Perhaps not elegant, we leave the physical dimensions of *length* in z and (*length*)^2 in w.

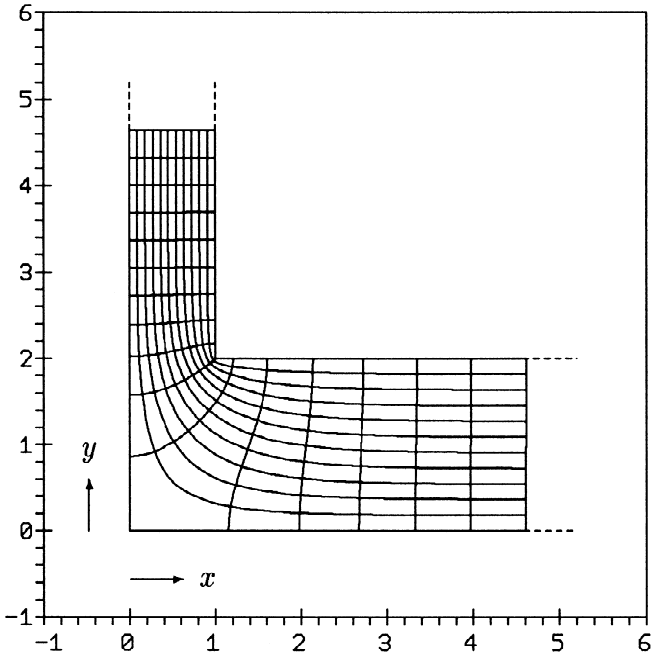

Figure 3. Equipotential and flux lines for a=1.0 mm, b=2.0 mm

$$\phi_0 = \tfrac{1}{2}V\frac{\dfrac{L_a}{a} - \dfrac{2}{\pi}\left(\dfrac{b}{a}\arctan\dfrac{b}{a} + \log 2 - \dfrac{1}{2}\log\Big(\dfrac{a}{b}+\dfrac{b}{a}\Big) - \dfrac{1}{2}\log\dfrac{b}{a}\right)}{\dfrac{L_a}{a} + \dfrac{L_b}{b} - \dfrac{2}{\pi}\left(\dfrac{a}{b}\arctan\dfrac{a}{b} + \dfrac{b}{a}\arctan\dfrac{b}{a} + \log 4 - \log\Big(\dfrac{a}{b}+\dfrac{b}{a}\Big)\right)}$$

$$\simeq \tfrac{1}{2}V\frac{L_a/a}{L_a/a + L_b/b}. \tag{3.11}$$

An example of the electric field thus obtained is depicted in the Figure 3. The corresponding heat-source distribution is given by Figure 4. For later use, we summarize the resulting behaviour of ϕ in the various regions of interest:

$$\left.\begin{aligned} \phi &= \phi_0 - \frac{q}{a}y \\ &\quad + \frac{q}{\pi}\Big(\log\frac{4a^2}{a^2+b^2} + \frac{2b}{a}\arctan\frac{b}{a}\Big) \\ |\nabla\phi|^2 &= \Big(\frac{q}{a}\Big)^2 \end{aligned}\right\} \; y\to\infty,\ 0\le x\le a, \tag{3.12}$$

$$\left.\begin{aligned} \phi &= \phi_0 + \frac{q}{b}x \\ &\quad - \frac{q}{\pi}\Big(\log\frac{4b^2}{a^2+b^2} + \frac{2a}{b}\arctan\frac{a}{b}\Big) \\ |\nabla\phi|^2 &= \Big(\frac{q}{b}\Big)^2 \end{aligned}\right\} \; x\to\infty,\ 0\le y\le b, \tag{3.13}$$

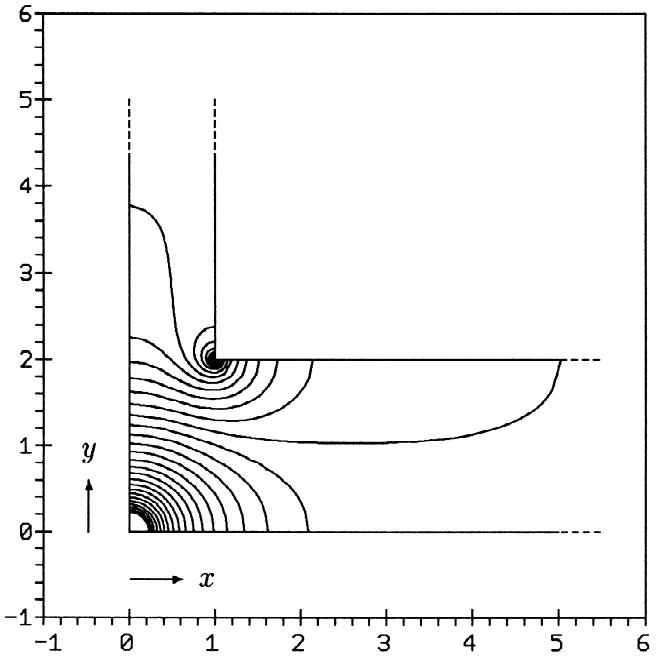

Figure 4. Contours of constant source strength for a=1.0 mm, b=2.0 mm

$$\left.\begin{aligned} \phi &= \phi_0 + \frac{2q}{\pi}\log\frac{a}{b} \\ &\quad -\frac{q}{\pi}\Big(\frac{1}{a^2}+\frac{1}{b^2}\Big)^{1/3}(\tfrac{3}{2}\pi r)^{2/3}\cos(\tfrac{2}{3}\theta-\tfrac{1}{3}\pi) \\ |\nabla\phi|^2 &= q^2\Big(\frac{1}{a^2}+\frac{1}{b^2}\Big)^{2/3}(\tfrac{3}{2}\pi r)^{-2/3} \end{aligned}\right\} \quad \begin{aligned} &x+\mathrm{i}y = a+\mathrm{i}b+r\mathrm{e}^{\mathrm{i}\theta}, \\ &r\to 0,\ \ \tfrac{1}{2}\pi\le\theta\le 2\pi, \end{aligned} \tag{3.14}$$

$$\left.\begin{aligned} \phi &= \phi_0 + \frac{\pi q}{4}\frac{r^2\cos 2\theta}{a^2+b^2} \\ |\nabla\phi|^2 &= \frac{\pi^2 q^2}{4(a^2+b^2)^2}r^2 \end{aligned}\right\} \quad \begin{aligned} &x+\mathrm{i}y = r\mathrm{e}^{\mathrm{i}\theta}, \\ &r\to 0,\ 0\le\theta\le\tfrac{1}{2}\pi. \end{aligned} \tag{3.15}$$

These equations together define a conformal map from the physical (x,y)-plane to the electrostatic field (ϕ,ψ)-plane (Figure 2). Since ϕ and ψ both satisfy Laplace's equation, and are related by the Cauchy-Riemann equations

$$F'(z) = \psi_x + \mathrm{i}\psi_x = -\mathrm{i}\phi_y + \psi_y, \tag{3.16}$$

we have

$$|F'(z)|^2 = |\nabla\phi|^2, \tag{3.17}$$

which is not only σ^{-1} times the heat-source distribution, but also just the inverse of the Jacobian of the mapping $(x,y)\to(\phi,\psi)$, *i.e.*

$$|\nabla\phi|^2\mathrm{d}x\mathrm{d}y = \mathrm{d}\phi\mathrm{d}\psi. \tag{3.18}$$

Since practical evaluation will be needed later on, it may be useful to note that

$$|\nabla\phi|^2 = \frac{q^2}{ab}\sqrt{\frac{\cosh(u-\log b^2)-\cos v}{\cosh(u-\log a^2)+\cos v}}, \tag{3.19}$$

where $u+\mathrm{i}v = \pi q^{-1}(F-\phi_0)+\log b^2$.

4. The initial-value problem

At the start of the soldering process the electric heat source dominates the effect of thermal diffusion in most of the thermode. Hence, the source is only balanced by the energy storage term $\rho c\frac{\partial T}{\partial t}$. This is because a smooth behaviour of $|\nabla\phi|$ results (except for the vicinity of the cold end I) in a smooth temperature profile with a small diffusion term $\nabla^2 T$. This is particularly true for the legs, where $\nabla\phi$ is constant. So, initially, we have four domains to consider:

a) A region with a smoothly behaving $\nabla\phi$, not close to the cold end, where the temperature increase is directly coupled to the source, with only a secondary role for diffusion.

b) The cold end I where the temperature boundary condition $T = T_0$ creates a steep temperature gradient, giving a heat diffusion of equal importance as heat-up and source terms. It is of practical interest to know after what time the diffusion of the low end-temperatures reduces the temperature increase in the thermode.

c) At the inner corner (a, b) the source $|\nabla\phi|^2$ has a singularity of the order $O(r^{-2/3})$ (where r is the distance to the corner) which creates locally an intense temperature rise, so that diffusion and the other terms become equally important. The initial temperature overshoot at the corner diffuses away after some time. It is of practical interest to know if this time is less than the total heat-up time.

d) At the outer corner $(0, 0)$ the source $|\nabla\phi|^2$ has a behaviour of the type $O(r^2)$ which corresponds to a vanishing heat source and, therefore, also in this case a diffusion term which is of equal importance as the the other terms. So we may expect that at the very beginning of the process, this corner is slightly colder than the rest of the thermode. Then, the hot inner corner becomes effective and heats up the whole corner region, until this is again reduced by the cooling effect of the end.

a) THE MAIN DOMAIN

The fact that the diffusion term in Equation (2.3) is of secondary importance suggests an iterative process to construct a solution. Assuming a vanishing zeroth order solution $T_0(x, y, t) \equiv 0$, we can construct formally higher-order approximations by:

$$\rho c\frac{\partial T_n}{\partial t} = k\nabla^2 T_{n-1} + \sigma|\nabla\phi|^2, \tag{4.1}$$

which, in view of the source being independent of time, readily results into the following (formal) solution

$$\begin{aligned} T(x, y, t) &= T_0 + \frac{\sigma}{k}\sum_{n=1}\frac{1}{n!}\Big(\frac{kt}{\rho c}\Big)^n \nabla^{2(n-1)}(|\nabla\phi|^2) \\ &= T_0 + \frac{\sigma}{\rho c}|\nabla\phi|^2 t + \cdots. \end{aligned} \tag{4.2}$$

In general, this result is only to be interpreted in some asymptotic sense for small time. Obviously, it is neither valid for all t nor for all $\mathbf{x}$, since none of the boundary conditions is explicitly applied. Nevertheless, in a practical situation of heating up a thermode as quickly as possible, we are at start-up usually in this "small-time" regime for the main part of the thermode. Only near end I and the corners, solution (4.2) is not valid. Consider, for example, end II. Using (3.13) we have

$$T(L_b, 0, t) = T_0 + \frac{\sigma}{\rho c}\Big(\frac{q}{b}\Big)^2 t. \tag{4.3}$$

This may be compared with an "exact" numerical solution of the present problem, (2.4) and (2.3) in (2.7) with (2.8–2.10) and (2.11). This solution has been generated by the finite-element package SEPRAN ([16]), as described in Appendix C. In Figure 5 the temperature is shown at

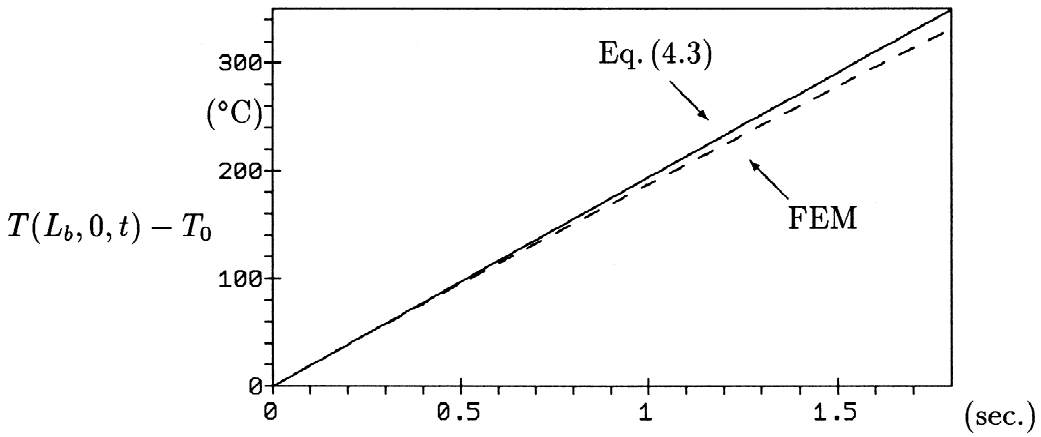

Figure 5. Temperature at $x = L_b$ and $y = 0$

$x = L_b$ and $y = 0$ for a thermode of molybdenum with $V = 0.4\,\mathrm{V}$, $L_a = 20\,\mathrm{mm}$, $L_b = 10\,\mathrm{mm}$ and $a = b = 2\,\mathrm{mm}$. The similarity between the analytical and numerical solutions is very good.

Under the assumption that the influence of cold end I has not yet reached the end II, we can use the above result to estimate the total heat-up time. It is found that the temperature T_∞ is reached after the total heat-up time

$$t_{\text{heat-up}} = \frac{\rho c}{\sigma}\Big(\frac{b}{q}\Big)^2 (T_\infty - T_0). \tag{4.4}$$

For the above example, with $T_\infty - T_0 = 275°\mathrm{C}$, this gives 1.42 s (numerically: 1.48 s) for molybdenum, 1.72 s for tungsten, and 24.4 s for Hastelloy.

Note that in leg I and leg II the source strengths are not equal, but have a ratio of a^2/b^2. This means that when a and b differ in any substantial way, a temperature gradient across the corner region is built up, which, after some time, will be levelled off by a flow of heat from one leg to the other. This effect will not be considered here.

b) THE COLD END

Near the end I the heat source is constant: $|\nabla\phi|^2 = (q/a)^2$ (Equation 3.12). Also, the boundary and initial-value conditions are uniform: $T = T_0$ at $y = L_a$ and $t = 0$. This implies that the solution is only a function of y and t, so that Equation (2.3) reduces to

$$\rho c \frac{\partial T}{\partial t} = k \frac{\partial^2 T}{\partial y^2} + \sigma \left(\frac{q}{a}\right)^2 \tag{4.5}$$

This equation may be solved by the similarity solution

$$\left.\begin{aligned} T(x,y,t) &= T_0 + \frac{\sigma}{\rho c}\left(\frac{q}{a}\right)^2 t f(\eta), \\ \eta^2 &= \frac{\rho c}{4kt}(L_a - y)^2 \\ f(\eta) &= (1+2\eta^2)\ \mathrm{erf}(\eta) + \frac{2}{\sqrt{\pi}}\eta\, \mathrm{e}^{-x^2} - 2\eta^2 \\ \mathrm{erf}(\eta) &= \frac{2}{\sqrt{\pi}} \int_0^\eta \mathrm{e}^{-t^2} \mathrm{d}t \end{aligned}\right\} \tag{4.6}$$

The behaviour of f is graphically described by Figure 6. For small time t and large η,

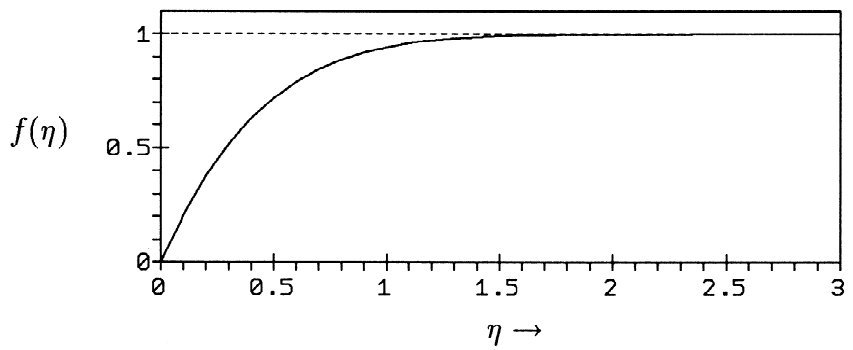

Figure 6. Scaled transient temperature near edge $y = L_a$

the shape function $f \simeq 1$, so that the temperature behaves like in the "main domain" as $T = T_0 + (\sigma/\rho c)|\nabla\phi|^2 t$. When at a fixed position y the time t increases, the similarity variable η decreases. For t so large that $\eta \leq O(1)$, f reduces to values smaller than 1, diminishing the growth of T. So, in this way the effect of the cold end I is felt at the corner ($y \sim 0$) after a diffusion time

$$t_{\text{cold-end}} \geq \frac{\rho c}{4k} L_a^2. \tag{4.7}$$

For the above example, with $L_a = 20$ mm, this yields 2.34 s for molybdenum, 1.92 s for tungsten, and 26.0 s for Hastelloy.

c) THE SINGULAR INNER CORNER (A,B).

It is seen from from Equation (3.14) that near the corner (a, b) the heat source is a function of r (the distance to the corner) only, and behaves like $|\nabla\phi|^2 = O(r^{-2/3})$. Also the boundary conditions $\partial T/\partial\theta = 0$ at $\theta = \frac{1}{2}\pi$ and 2π do not give rise to any dependence of T on

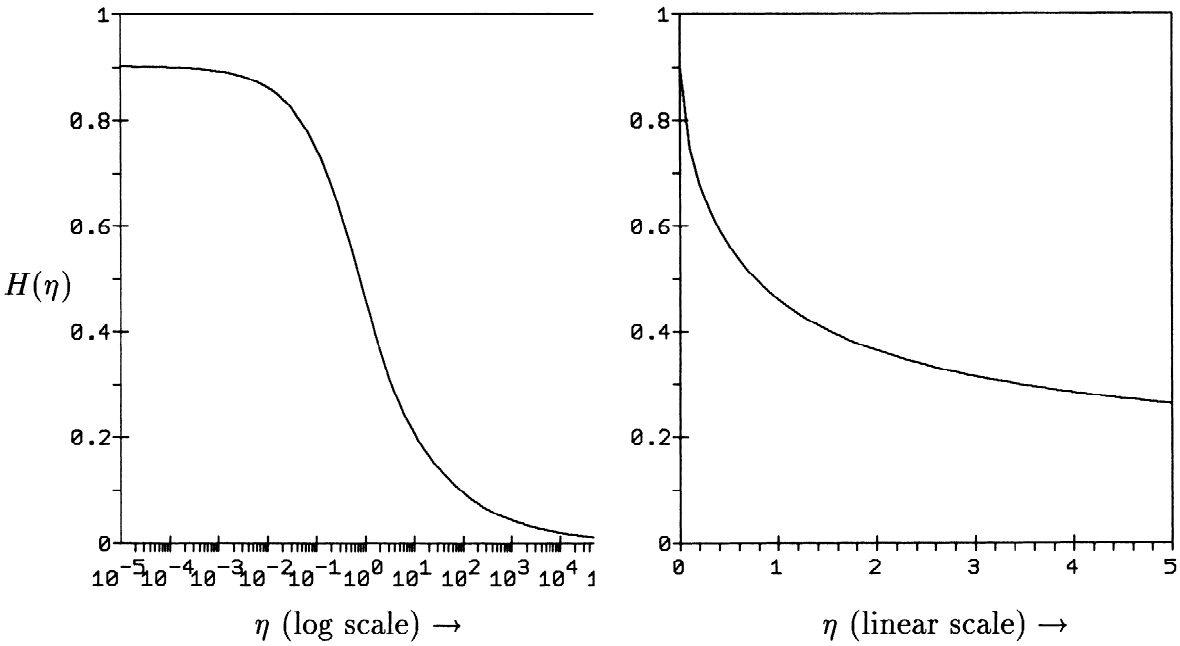

Figure 7. Scaled temperature $H(\eta)$ near inner corner a, b

θ, the angular coordinate in the corner. Therefore, T is a function of r and t only, so that Equation (2.3) reduces to

$$\rho c\frac{\partial T}{\partial t} = k\Big(\frac{\partial^2 T}{\partial r^2} + \frac{1}{r}\frac{\partial T}{\partial r}\Big) + \sigma q^2\Big(\frac{1}{a^2}+\frac{1}{b^2}\Big)^{2/3}(\tfrac{3}{2}\pi r)^{-2/3}. \tag{4.8}$$

This equation has the following similarity solution (see Appendix B)

$$\left.\begin{aligned} T(x,y,t) &= T_0 + \frac{\sigma}{k}q^2\Big(\frac{1}{a^2}+\frac{1}{b^2}\Big)^{2/3}\Big(\frac{9kt}{8\pi\rho c}\Big)^{2/3}H(\eta)\\ H(\eta) &= \Gamma(\tfrac{5}{3})\,{}_1F_1(-\tfrac{2}{3};1;-\eta^2) - \eta^{4/3}\\ \eta^2 &= \frac{\rho c r^2}{4kt} \end{aligned}\right\} \tag{4.9}$$

where ${}_1F_1(a;b;z)$ is the confluent hypergeometric function. A graphical description of the shape function $H(\eta)$ as a function of η is given in Figure 7. As is shown in Appendix B, this solution perfectly matches to the far-field "main-domain" behaviour for large r (large η). The most important property of (4.9) is the value at the corner:

$$T(a,b,t) = T_0 + \Gamma(\tfrac{5}{3})\Big(\frac{9}{8\pi}\Big)^{2/3}\frac{\sigma}{k}q^2\Big(\frac{1}{a^2}+\frac{1}{b^2}\Big)^{2/3}\Big(\frac{kt}{\rho c}\Big)^{2/3} \tag{4.10}$$

When we compare this value with the far field (the average value between leg I and leg II, for subjective reasons of symmetry), we may obtain an estimate for the time it takes before the temperature overshoot at the corner is dissipated away. The ratio

$$\frac{T(a,b,t)-T_0}{\frac{1}{2}(T(I)+T(II))-T_0} = \frac{\Gamma(\frac{5}{3})}{2}\Big(\frac{9}{\pi}\Big)^{2/3}\Big(\frac{1}{a^2}+\frac{1}{b^2}\Big)^{-1/3}\Big(\frac{kt}{\rho c}\Big)^{-1/3}$$

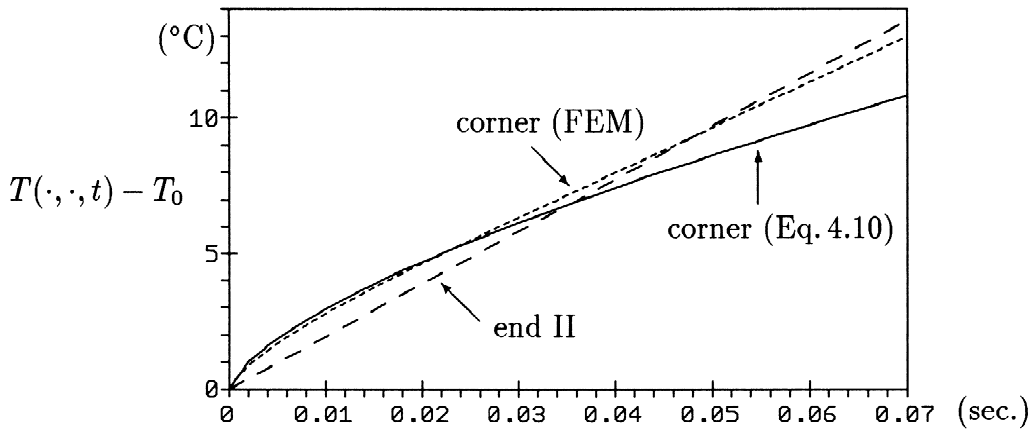

Figure 8. Temperature at corner (a,b) and at end II

is numerically smaller than 1 when t is larger than the *corner excess diffusion time*

$$t_{\text{ced}} = \frac{81\Gamma(\frac{5}{3})^3}{8\pi^2}\frac{\rho c}{k}ab\Big(\frac{a}{b}+\frac{b}{a}\Big)^{-1} = 0.7547\,\frac{\rho c}{k}ab\Big(\frac{a}{b}+\frac{b}{a}\Big)^{-1} \tag{4.11}$$

For the above example, with $a = b = 2\,\text{mm}$, this is 0.035 s for molybdenum, 0.029 s for tungsten, and 0.39 s for Hastelloy. Apparently, for the values selected here the temperature overshoot does not exist long enough for it to be of any importance.

All this is very well confirmed by the same finite-element "exact" solution discussed above (molybdenum with $V = 0.4\,\text{V}, L_a = 20\,\text{mm}, L_b = 10\,\text{mm}$ and $a = b = 2\,\text{mm}$; Appendix C). In Figure 8 the temperature near the corner $x = a$, $y = b$, (both the numerical and the analytical one) is compared with the far field (at end II). After about 0.04 seconds the corner temperature does not dominate any longer over the far-field temperature.

d) THE SMOOTH OUTER CORNER (0,0).

In a way, this is rather similar to the inner corner. Again, the source is a function of r only, although now a very smooth one: $|\nabla\phi|^2 = O(r^2)$, as given by Equation (3.15). Also, the boundary conditions are such that T is a function of r and t only, so that Equation (2.3) reduces to

$$\rho c\frac{\partial T}{\partial t} = \frac{k}{r}\frac{\partial}{\partial r}\Big(r\frac{\partial T}{\partial r}\Big) + \frac{\sigma\pi^2 q^2}{4(a^2+b^2)^2}r^2. \tag{4.12}$$

This equation is also of the type solved in Appendix B; however, the confluent hypergeometric function now simplifies greatly, since ${}_1F_1(-2;1;z) = 1 - 2z + \frac{1}{2}z^2$, and we obtain

$$T(x,y,t) = T_0 + \frac{\sigma\pi^2 q^2}{4(\rho c)^2(a^2+b^2)^2}(2kt^2 + \rho c r^2 t). \tag{4.13}$$

Due to its zero source strength, the corner is only heated by conduction from its neighbourhood. If the distance between the corners $(0,0)$ and (a,b) is large enough, *i.e.* if $\eta^2 = \rho c(a^2 + b^2)/4kt_{\text{ced}}$ (see Equation 4.9) is large enough, the corner $(0,0)$ is never heated by corner (a,b) more than by the far fields $T(I)$ or $T(II)$. In that case, the corner temperature that starts as a

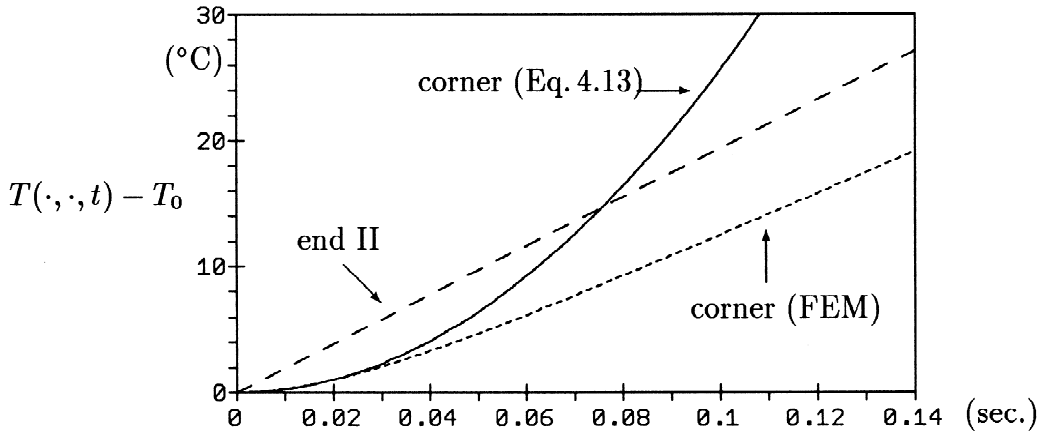

Figure 9. Temperature at corner (0,0) and at end II

quadratic function in time (Equation 4.13), will after some time, the *corner shortage diffusion time* t_{csd}, become comparable with the far field, and then gradually change into some linear-type growth that follows the far field. As a result, not only the temperature $T(0,0,t)$ itself, but also its slope $\partial T(0,0,t)/\partial t$ will never exceed the far field counterparts. An estimate of this corner-shortage diffusion time is therefore the time it takes before approximation (4.13) and the far field have the same slope:

$$\frac{\partial T(0,0,t)}{\partial t} = \frac{1}{2}\frac{\partial (T(I) + T(II))}{\partial t}$$

which results in

$$t_{\text{csd}} = \frac{1}{2\pi^2}\frac{\rho c}{k} ab\Big(\frac{a}{b} + \frac{b}{a}\Big)^3. \tag{4.14}$$

This is equal to or larger than t_{ced}, as we have the ratio

$$\frac{t_{\text{csd}}}{t_{\text{ced}}} = \frac{4}{81\Gamma(\frac{5}{3})^3}\Big(\frac{a}{b} + \frac{b}{a}\Big)^4 = \frac{1}{14.90}\Big(\frac{a}{b} + \frac{b}{a}\Big)^4,$$

which for $a/b = 1$ is equal to 1.07, and larger otherwise.

These observations may be confirmed by comparison with the numerical FEM-solution, introduced earlier (molybdenum with $V = 0.4\,\text{V}$, $L_a = 20\,\text{mm}$, $L_b = 10\,\text{mm}$ and $a = b = 2\,\text{mm}$). In Figure 9 the analytical expression (4.13) for the temperature at the corner $x = 0$, $y = 0$ is compared with its numerical counterpart, and the "far-field" temperature at end II. We see indeed that after about 0.04 sec. the corner temperature tends to follow the far field.

5. The stationary problem

In the previous section we dealt with the first question, *i.e.* how to keep the excess temperature in the corner below the end temperature. Now we will consider the second question of a uniform temperature distribution in the stationary problem.

After the final temperature T_∞ at end II has been reached, heating will be reduced to just the amount necessary to maintain this temperature, *i.e.* the electric potential difference V

is turned down to a small value. After a short time the temperature will be stationary, and Equation (2.3) reduces to

$$k\nabla^2 T + \sigma|\nabla\phi|^2 = 0. \tag{5.1}$$

The second question concerning the uniformity of the temperature can now be answered by an exact solution. As was explained above, there is even an exact solution for the more general case of temperature-dependent conductivities. We will assume here a constant k and a σ satisfying relation (2.6). The electric potential now satisfies Equation (2.1).

a) THE EXACT SOLUTION

As was observed by Young [4, 9], the parallel boundary conditions to T and ϕ imply that T may be written as a function of ϕ only: $T = T(\phi)$. After elimination of $\nabla^2\phi$ and $|\nabla\phi|^2$ we obtain the equation

$$\Big(\frac{k}{\sigma}\Big)^2 \frac{\mathrm{d}^2 T}{\mathrm{d}\phi^2} + \frac{1}{2}\Big(\frac{\mathrm{d}T}{\mathrm{d}\phi}\Big)^2 \frac{\mathrm{d}}{\mathrm{d}T}\Big(\frac{k}{\sigma}\Big)^2 + \frac{k}{\sigma} = 0. \tag{5.2}$$

Since ϕ increases monotonically from end I to end II, the boundary conditions in terms of ϕ are now

$$T(0) = T_0, \qquad T'(\tfrac{1}{2}V) = 0. \tag{5.3}$$

Since $k/\sigma = k\beta(T - T_1)$, we can solve this equation as follows:

$$T(\phi) = T_1 + \sqrt{(T_0 - T_1)^2 - (\phi^2 - \phi V)/k\beta}. \tag{5.4}$$

For linear material ($\sigma = \sigma_0$ constant) this would be

$$T(\phi) = T_0 + \frac{\sigma_0}{2k}(\phi V - \phi^2), \tag{5.5}$$

and we would have completed our task, because we already have the electric field ϕ, as found in section 3. For the nonlinear case our task will be slightly more involved, but, as it happens, we can still use this linear field. Note that the above relations between temperature and electric field are valid for *any* geometry, with insulated boundaries and two sides with a given constant potential and temperature. The linear result was given in Carslaw and Jaeger (ref. [6, ch. 4.10]) for the one-dimensional problem of a thin wire heated by an electric current.

Let us introduce the auxiliary potential Φ which satisfies

$$\sqrt{\frac{k}{\beta}}\,\nabla\Phi = \sigma(T)\nabla\phi.$$

The functions T and ϕ can be expressed in terms of Φ

$$\begin{aligned}
\phi &= \tfrac{1}{2}V + \sqrt{k\beta}(T_0 - T_1)\sin\Phi - \tfrac{1}{2}V\cos\Phi, \\
T &= T_1 + (T_0 - T_1)\cos\Phi + \frac{\frac{1}{2}V}{\sqrt{k\beta}}\sin\Phi.
\end{aligned}$$

while Φ satisfies Laplace's equation with boundary conditions

$$\Phi = 0 \qquad \text{at end I,} \tag{5.6}$$

$$\Phi = \Phi_{\frac{1}{2}V} = \arctan\Big(\frac{\frac{1}{2}V}{\sqrt{k\beta}(T_0 - T_1)}\Big) \qquad \text{at end II,} \tag{5.7}$$

$$\nabla\Phi \cdot \mathbf{n} = 0 \qquad \text{at the insulated boundaries.} \tag{5.8}$$

In other words, Φ is equal to ϕ with constant σ (Section 3), but with $\Phi_{\frac{1}{2}V}$ instead of $\frac{1}{2}V$. The constant Q, corresponding to q of Equation (3.10), now becomes

$$Q \simeq \frac{1}{L_a/a \,+\, L_b/b} \arctan\Big(\frac{\frac{1}{2}V}{\sqrt{k\beta}(T_0 - T_1)}\Big), \tag{5.9}$$

and the constant Φ_0, corresponding to ϕ_0 of Equation (3.11), becomes

$$\Phi_0 \simeq \frac{L_a/a}{L_a/a \,+\, L_b/b} \arctan\Big(\frac{\frac{1}{2}V}{\sqrt{k\beta}(T_0 - T_1)}\Big). \tag{5.10}$$

A graphical description of a possible temperature field is given in the Figure 10.

Now we are able to compare the temperature at the center of the lower bar (end point II) with the outer corner (0,0). These points correspond with $\Phi = \Phi_{\frac{1}{2}V}$ ($\phi = \frac{1}{2}V$) and $\Phi = \Phi_0$ ($\phi = \phi_0$), respectively. So, under the usual approximation of large L_a/a and L_b/b, we obtain the ratio

$$\frac{T(0,0)}{T(L_b,0)} \;=\; \frac{T(\Phi=\Phi_0)}{T(\Phi=\Phi_{\frac{1}{2}V})} = \frac{T_1 + \sqrt{(T_0-T_1)^2 + \frac{1}{4}V^2/k\beta}\,\cos(\lambda\Phi_{\frac{1}{2}V})}{T_1 + \sqrt{(T_0-T_1)^2 + \frac{1}{4}V^2/k\beta}}, \tag{5.11}$$

where

$$\lambda = \frac{L_b/b}{L_a/a + L_b/b}.$$

This temperature ratio (5.11) along leg II is never equal to unity. However, we can make the difference with 1 as small as we wish by selecting a geometry such that λ is small enough.

As might be expected, this conclusion would be entirely the same if we would consider a linear material. When the temperature along leg II becomes constant, the material properties become constant as well.

b) THE TOTAL LINEAR AND NONLINEAR SOURCE STRENGTHS

An interesting result for comparing the linear approximation and the full nonlinear model, *e.g.* for selecting a representative value of σ_0, is the ratio between the total source strengths $\int\!\!\int_{\Omega_L} \sigma|\nabla\phi|^2 \,\mathrm{d}x\mathrm{d}y$.

We may evaluate this integral analytically, both in the linear and the nonlinear cases, by using the fact that $|\nabla\phi|^2$ and $|\nabla\Phi|^2$ are the inverses of the Jacobian of the transformations of (x,y) to (ϕ,ψ) and (Φ,Ψ), respectively (Ψ is the conjugate of Φ). So we find

$$\frac{\int\!\!\int_{\Omega_L} \sigma(T)|\nabla\phi|^2 \,\mathrm{d}x\mathrm{d}y}{\int\!\!\int_{\Omega_L} \sigma_0|\nabla\phi|^2 \,\mathrm{d}x\mathrm{d}y} = \frac{k\int\!\!\int_{\Omega_L} (T-T_1)|\nabla\Phi|^2 \,\mathrm{d}x\mathrm{d}y}{\sigma_0\int\!\!\int_{\Omega_L} |\nabla\phi|^2 \,\mathrm{d}x\mathrm{d}y}$$

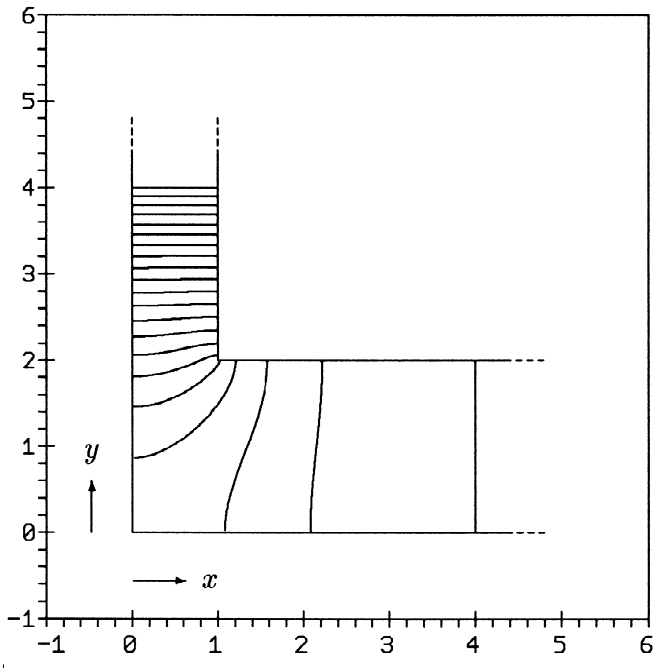

Figure 10. Contours of constant temperature for a=1.0 mm, b=2.0 mm, L_a=L_b=4.0 mm

$$= \frac{kQ\int_0^{\Phi_{\frac{1}{2}V}} (T - T_1)\,\mathrm{d}\Phi}{\frac{1}{2}V\sigma_0 q} = \frac{\frac{1}{2}VkQ/\sqrt{k\beta}}{\frac{1}{2}V\sigma_0 q} = \frac{\sigma(T_0)}{\sigma_0}\frac{\Phi_{\frac{1}{2}V}}{\tan\Phi_{\frac{1}{2}V}}. \tag{5.12}$$

(Note that $\Phi_{\frac{1}{2}V}/\tan\Phi_{\frac{1}{2}V} < 1$.) So the value for σ_0, such that the integrated source strengths in both the linear and the nonlinear models are the same, is equal to

$$\sigma_0 = \sigma(T_0)\frac{\Phi_{\frac{1}{2}V}}{\tan\Phi_{\frac{1}{2}V}}.$$

6. Conclusions

The nonuniform heating problem of a ⊔-shaped thermode may be split up into the following parts. During the initial dynamic phase the material heats up in close agreement with the (nonuniform) source distribution. This leads to a uniform temperature in the straight parts, an overshoot near the inner corners where the electric field is singular, and a lower temperature near the outer corners where the electric field vanishes. This distribution, together with the cold boundary condition at the cool ends, induces a local heat flux which does not balance the source, so the temperature will move in time to its stationary equilibrium. The times involved in this redistribution may be used to select the problem parameters such that the undesired overshoot is controlled:

the corner excess diffusion time

$$t_{\text{ced}} = \frac{81\Gamma(\frac{5}{3})^3}{8\pi^2}\frac{\rho c}{k}ab\Big(\frac{a}{b} + \frac{b}{a}\Big)^{-1} = 0.7547\,\frac{\rho c}{k}ab\Big(\frac{a}{b} + \frac{b}{a}\Big)^{-1}$$

should be smaller than the total heat-up time

$$t_{\text{heat-up}} = \frac{\rho c}{\sigma}\Big(\frac{b}{q}\Big)^2(T_\infty - T_0)$$

or larger than the cold-end diffusion time

$$t_{\text{cold-end}} \geq \frac{\rho c}{4k}L_a^2$$

for the corner overshoot to be negligible.

The other part of the nonuniform heating problem is the stationary problem. The cold ends cool off the thermode in such a way that the corners may become too cold. On the other hand, the same corners induce a locally intense electric field that may compensate for this effect, so as to keep the corners and the rest of the bar meant for soldering at an almost uniform temperature. We obtain this almost uniform temperature by selecting the geometry such that

$$\frac{L_b/b}{L_a/a + L_b/b} \quad \text{is small enough.}$$

Appendix A. Conformal mapping of polygonal boundaries

According to the Schwarz-Christoffel theorem ([14, 15]), a polygonal boundary in the complex z-plane with interior angles $\nu_1, \nu_2, \nu_3, \ldots$ is mapped onto the real axis $\mathrm{Im}(w) = 0$ of the complex w-plane by the transformation $z = z(w)$, given by

$$\frac{\mathrm{d}w}{\mathrm{d}z} = K(w-p_1)^{1-\nu_1/\pi}\,(w-p_2)^{1-\nu_2/\pi}\,(w-p_3)^{1-\nu_3/\pi}\ldots \tag{A.1}$$

where K is a constant and $p_1, p_2, p_3, \ldots$ are the real values of w corresponding to the vertices of the polygon. The region in the w-plane corresponding to the polygonal interior is the half-plane $\mathrm{Im}(w) > 0$. The interior angle of a vertex at infinity is zero. One such point may be mapped to infinity in the w-plane, with K tending to zero at the same time, such, that the factor $K(w - w_1)$ is effectively constant.

In the present problem for Ω_∞ the following equation is selected

$$\frac{\mathrm{d}w}{\mathrm{d}z} = \frac{\pi\mathrm{i}}{b}\frac{w\sqrt{b^2-w}}{\sqrt{a^2+w}}. \tag{A.2}$$

with solution $z = G(w)$ given by

$$\begin{aligned} G(w) &= \frac{2\mathrm{i}a}{\pi}\,\mathrm{artanh}\left(\frac{a\sqrt{b^2-w}}{b\sqrt{a^2+w}}\right) + \frac{2\mathrm{i}b}{\pi}\arctan\left(\frac{\sqrt{b^2-w}}{\sqrt{a^2+w}}\right) \\ &= \frac{a\mathrm{i}}{\pi}\log\left(\frac{b\sqrt{a^2+w}+a\sqrt{b^2-w}}{b\sqrt{a^2+w}-a\sqrt{b^2-w}}\right) - \frac{b}{\pi}\log\left(\frac{\mathrm{i}\sqrt{a^2+w}+\sqrt{b^2-w}}{\mathrm{i}\sqrt{a^2+w}-\sqrt{b^2-w}}\right) \end{aligned} \tag{A.3}$$

The interior angles to be dealt with are 0 and 0 in the legs at infinity, $\frac{1}{2}\pi$ at $(0,0)$, and $\frac{3}{2}\pi$ at (a,b). The infinite vertex $y \to \infty,\ 0 \leq x \leq a$ is mapped to $w = 0$, the infinite vertex $x \to \infty,\ 0 \leq y \leq b$ to $w \to \infty$. The real values corresponding to the other vertices are most conveniently taken to be b^2 and $-a^2$, so that

$$G(b^2) = 0 \quad \text{and} \quad G(-a^2) = a + \mathrm{i}b$$

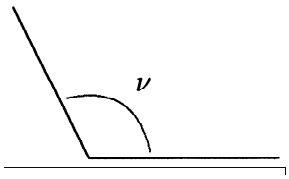

Figure 11. Wedge-shaped region

where the limit $\mathrm{Im}(w) \downarrow 0$ is understood. The definitions for log, square root, arctan, and artanh are the principal values, with

$$\arctan(x) = \frac{\mathrm{i}}{2}\log\frac{\mathrm{i}+x}{\mathrm{i}-x}, \quad \operatorname{artanh}(x) = \frac{1}{2}\log\frac{1+x}{1-x}.$$

The combined branch cuts of the square roots and the logarithms cause G to have branch cuts along $(-\infty, 0]$ and $[b^2, \infty)$. The boundary $\partial\Omega_\infty$ is mapped to the real w-axis as follows:

$$\begin{aligned}
&x > a,\ y = b \quad \text{for} \quad -\infty \le w \le -a^2,\\
&x = a,\ y > b \quad \text{for} \quad -a^2 \le w \le 0,\\
&x = 0,\ y > 0 \quad \text{for} \quad 0 \le w \le b^2,\\
&x > 0,\ y = 0 \quad \text{for} \quad b^2 \le w \le \infty.
\end{aligned}$$

The behaviour of G near the vertices is given by the asymptotic expressions

$$\left.\begin{aligned}
G(w) &\simeq \frac{b}{\pi}\left(\log\frac{w}{ab} + \log\frac{4ab}{a^2+b^2} + \frac{2a}{b}\arctan\frac{a}{b}\right) && (w\to\infty; x\to\infty)\\
G(w) &\simeq \frac{\mathrm{i}a}{\pi}\left(\log\frac{ab}{w} + \log\frac{4ab}{a^2+b^2} + \frac{2b}{a}\arctan\frac{b}{a}\right) && (w\to 0; y\to\infty)\\
G(w) &\simeq \frac{2\mathrm{i}}{\pi b}\sqrt{a^2+b^2}\,\sqrt{b^2-w} && (w\to b^2; x,y\to 0,0)\\
G(w) &\simeq a + \mathrm{i}b + \frac{2\mathrm{i}b}{3\pi a^2}\frac{(a^2+w)^{3/2}}{\sqrt{a^2+b^2}} && (w\to -a^2; x,y\to a,b)
\end{aligned}\right\} \quad \text{(A.4)}$$

Appendix B. The general initial-value problem in a corner

Consider the constant-σ, wedge-shaped two-dimensional region $0 \le \theta \le \nu$ with an electric field with complex potential $F(z) \sim z^{\pi/\nu}$, so that the potential of the field is

$$\phi(x,y) = (\nu/\pi) A\, r^{\pi/\nu}\cos(\theta\pi/\nu) \quad \text{(B.1)}$$

The temperature distribution T due to the heat generated by this field is then given by

$$\rho c\frac{\partial T}{\partial t} = k\nabla^2 T + \sigma A^2 r^{2\pi/\nu - 2} \quad \text{(B.2)}$$

with boundary conditions

$$\frac{\partial T}{\partial \theta} = 0 \quad \text{at } \theta = 0,\ \theta = \nu \quad \text{(B.3)}$$

and initial conditions

$$T(x,y,t) \equiv 0 \quad \text{at } t = 0. \quad \text{(B.4)}$$

Since there are no other (point) sources in $r = 0$, we have the additional condition of a finite field at the origin:

$$0 \le T(0,0,t) < \infty. \tag{B.5}$$

Boundary conditions and the symmetric source imply that T is a function of t and the radial coordinate r only, so that equation (B.2) reduces to

$$\rho c \frac{\partial T}{\partial t} = k\Big(\frac{\partial^2 T}{\partial r^2} + \frac{1}{r}\frac{\partial T}{\partial r}\Big) + \sigma A^2 r^{2\pi/\nu - 2}. \tag{B.6}$$

Dimensional analysis reveals that, owing to the homogeneous initial and boundary conditions, the infinite geometry, and the source being a monomial in r, homogeneous of the order $2\pi/\nu - 2$, there is no length scale in the problem other than $(kt/\rho c)^{1/2}$. This indicates that a similarity solution is possible. It appears that

$$T(r,t) = \frac{\sigma}{4k} A^2 \Big(\frac{4kt}{\rho c}\Big)^{\pi/\nu} h(X), \quad X = \frac{\rho c r^2}{4kt} \tag{B.7}$$

reduces Equation (B.6) to

$$Xh'' + (1+X)h' - (\pi/\nu)h = -X^{\pi/\nu - 1}. \tag{B.8}$$

This equation may be recognized as an inhomogeneous confluent hypergeometric equation in $-X$, which has the general solution

$$h(X) = C\,{}_1F_1(-\pi/\nu; 1; -X) + D\,U(-\pi/\nu, 1, -X) - (\nu/\pi)^2 X^{\pi/\nu} \tag{B.9}$$

where ${}_1F_1(a;b;z)$ and $U(a,b,z)$ are the regular and singular confluent hypergeometric functions (ref. [17, 18, 19]), which are solutions of Kummer's equation

$$zy'' + (b-z)y' - ay = 0. \tag{B.10}$$

Since U is singular at the origin:

$$U(-\pi/\nu, 1, -X) \simeq -\log(X)/\Gamma(-\pi/\nu) \quad (X \to 0) \tag{B.11}$$

this term has to vanish, and the integration constant D is equal to 0.

The function ${}_1F_1(a;b;z)$ is defined by

$${}_1F_1(a;b;z) = 1 + \frac{az}{b} + \frac{a(a+1)z^2}{b(b+1)2} + \cdots + \frac{(a)_n z^n}{(b)_n n!} + \cdots \tag{B.12}$$

where $(a)_n$ is Pochhammer's symbol, defined by

$$\begin{aligned} (a)_0 &= 1, \\ (a)_n &= a(a+1)(a+2)\cdots(a+n-1) = \frac{\Gamma(a+n)}{\Gamma(a)}. \end{aligned} \tag{B.13}$$

Note that for a equal to a negative integer, this series is finite and ${}_1F_1(a;b;z)$ is just a polynomial of order $-a$.

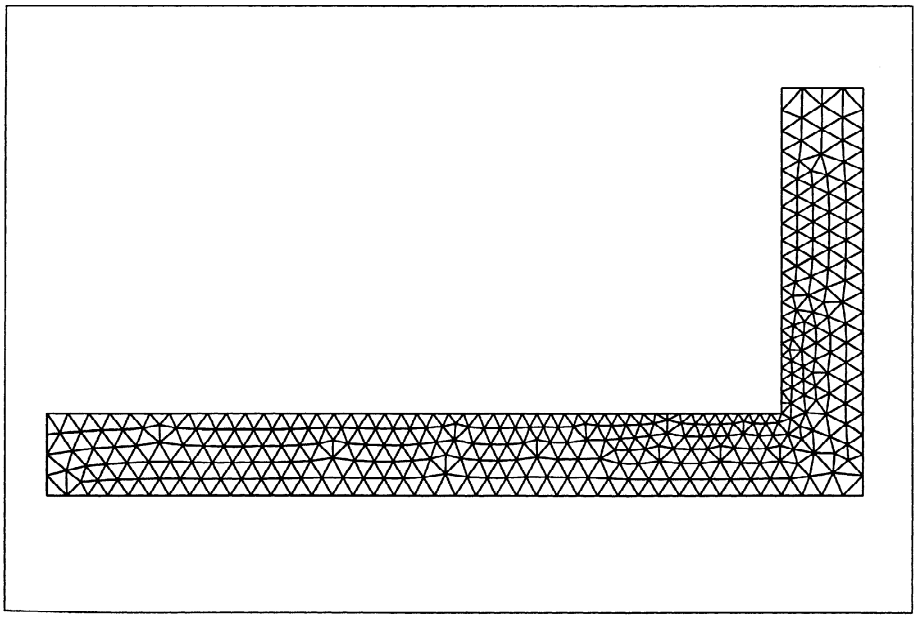

Figure 12. Mesh in the finite element calculation

${}_1F_1(-\pi/\nu;1;-X)$ has the asymptotic expansion

$$
\begin{aligned}
{}_1F_1(-\pi/\nu;1;-X) \;=\; & \frac{1}{\Gamma(1+\pi/\nu)}\sum_{n=0}^{R-1}\frac{((-\pi/\nu)_n)^2}{n!}X^{\pi/\nu-n} \\
& +O(X^{-R}) \qquad\qquad (X\to\infty)
\end{aligned}
\tag{B.14}
$$

so that the initial-value condition implies that the other integration constant is equal to

$$C=(\nu/\pi)\Gamma(\pi/\nu).$$

Putting everything together, we have the solution

$$
\begin{aligned}
T(x,y,t) \;&=\; \frac{\sigma\nu^2A^2}{4\pi^2k}\Big(\frac{4kt}{\rho c}\Big)^{\pi/\nu}\left[\Gamma\Big(1+\frac{\pi}{\nu}\Big){}_1F_1\Big(-\frac{\pi}{\nu};1;-\frac{\rho cr^2}{4kt}\Big)-\Big(\frac{\rho cr^2}{4kt}\Big)^{\pi/\nu}\right] \\
&=\; \frac{\sigma\nu^2A^2}{4\pi^2k}\left[\Big(\frac{4kt}{\rho c}\Big)^{\pi/\nu}\Gamma\Big(1+\frac{\pi}{\nu}\Big){}_1F_1\Big(-\frac{\pi}{\nu};1;-\frac{\rho cr^2}{4kt}\Big)-r^{2\pi/\nu}\right].
\end{aligned}
\tag{B.15}
$$

Note that, as expected, the behaviour for $r\to\infty$ ceases to depend on ∇^2T and is just a linear growth in time:

$$T(x,y,t)\simeq\frac{\sigma}{\rho c}A^2r^{2\pi/\nu-2}t \qquad\qquad (r\to\infty) \tag{B.16}$$

Finally, a remark may be in order about the effect of a finite radius of curvature of the corner that might occur in practice. In such a situation the present solution is not valid for very small time. This is seen as follows.

The present similarity solution is available because of the absence of any length scale in the problem. Therefore, the temperature has to depend on the inherent length scale $\ell=(4kt/\rho c)^{1/2}$. If we had a corner with a small but finite radius of, say, r_0, then a length scale

is introduced via the boundary condition $\partial T/\partial r = 0$ at $r = r_0$, which, strictly speaking, renders the present solution invalid. Indeed, for very short times, when $\ell \leq O(r_0)$, we need another solution. However, for larger times, the details of the corner become "invisible", and the present solution is valid.

APPENDIX C. FINITE-ELEMENT SOLUTION

By means of the finite-element package SEPRAN ([16]) a numerical solution of the present problem, (2.4) and (2.3) in (2.7) with (2.8–2.10) and (2.11), for a thermode of molybdenum with $V = 0.4\,\mathrm{V}$, $L_a = 20\,\mathrm{mm}$, $L_b = 10\,\mathrm{mm}$ and $a = b = 2\,\mathrm{mm}$, has been generated. The mesh used ultimately is given in Figure 12. By halving the mesh size from (typically) $\frac{1}{2}\,\mathrm{mm}$ to $\frac{1}{4}\,\mathrm{mm}$ and using an automatic time-step integrator with a relative accuracy of 10^{-3}, we estimated the typical relative accuracy of the solution to be less than $O(2 \cdot 10^{-3})$.

Acknowledgements:

The author gratefully acknowledges the enthusiastic support of J.K.M. Jansen and L.G.F.C. van Bree by programming and running the SEPRAN package for the present problem, and the interesting remarks by prof. J. Boersma.

References

1. L.D. Landau and E.M. Lifshitz, *Electrodynamics of Continuous Media*. Oxford: Pergamon Press (1960) 417 pp.
2. D.S. Jones, *The Theory of Electromagnetism*. Oxford: Pergamon Press (1964) 807 pp.
3. M. Mason and W. Weaver, *The Electromagnetic Field*. New York: Dover Publications Inc. (1929) 390 pp.
4. J.H. Young, Steady state Joule heating with temperature dependent conductivities. *Applied Scientific Research* 43 (1986) 55–65.
5. F. Kreith and M.S. Bohn, *Principles of Heat Transfer* (4th ed.). New York: Harper & Row (1986) 700 pp.
6. H.S. Carslaw and J.C. Jaeger, *Conduction of Heat in Solids* (2nd ed.). Oxford: Clarendon Press (1973) 510 pp.
7. R.E. Bolz and G.L. Tuve (eds.), *Handbook of tables for Applied Engineering Science* (2nd ed.). Cleveland (Ohio): The Chemical Rubber Company (1973) 1166 pp.
8. D.R. Lide (ed.), *CRC Handbook of Chemistry and Physics*. London: CRC Press Inc. (1994) 2531 pp.
9. J.H. Young, Quasi-linear electrical potentials in steady-state Joule heating. *Journal of Engineering Mathematics* 21 (1987) 33–40.
10. L. Lorenz, On the thermal and electrical conductivities of metals. *Ann. Physik Leipzig* 13(3) (1881) 422–447.
11. G.S. Kumar, G. Prasad, and R.O. Pohl, Experimental determinations of the Lorenz number. *Journal of Materials Science* 28(16) (1993) 4261–4272.
12. G. Cimatti, Remark on existence and uniqueness for the thermistor problem under mixed boundary conditions. *Quarterly of Applied Mathematics* 47(1) (1989) 117–121.
13. S.D. Howison, J.F. Rodrigues, and M. Shillor, Stationary Solutions to the Thermistor Problem. *Journal of Mathematical Analysis and Applications* 174 (1993) 573–588.
14. M.R. Spiegel, *Shaum's Outline Series of Theory and Problems of Complex Variables: with an Introduction to Conformal Mapping and its Applications*. New York: McGraw-Hill Inc. (1974) 313 pp.
15. M. Walker, *The Schwarz-Christoffel Transformation and Its Applications - A Simple Exposition*. New York: Dover Publications Inc. (1964) 116 pp.
16. A. Segal, *SEPRAN user manual, standard problems and programmers guide*. Leidschendam (The Netherlands): Ingenieursburo SEPRA (1984).
17. M. Abramowitz and I.A. Stegun (eds.), *Handbook of Mathematical Functions*. New York: National Bureau of Standards, Dover Publications, Inc. (1964) 1045 pp.
18. A. Erdelyi, W. Magnus, F. Oberhettinger, and F.G. Tricomi, *Higher Transcendental Functions, Volume 1*. New York: McGraw-Hill Book Company, Inc. (1953) 302 pp.
19. I.S. Gradshteyn, and I.M. Ryzhik, *Table of Integrals, Series and Products* (5th ed.). Edited by A. Jeffrey, London: Academic Press (1994) 1204 pp.